

Spin Current Density Functional Theory of the Quantum Spin-Hall Phase

William P. Comaskey,¹ Filippo Bodo,^{2,3} Alessandro Erba,^{2,*}

Jose L. Mendoza-Cortes,^{1,4,†} and Jacques K. Desmarais^{2,‡}

¹*Department of Physics, College of Arts and Science,
Florida State University, Tallahassee FL, 32310, USA.*

²*Dipartimento di Chimica, Università di Torino, Via Giuria 5, 10125 Torino, Italy*

³*Department of Chemistry, Southern Methodist University, Dallas, Texas, USA*

⁴*Department of Chemical Engineering & Materials Science,
Michigan State University, East Lansing, Michigan 48824, United States.*

(Dated: August 31, 2022)

The spin current density functional theory (SCDFT) is the generalization of the standard DFT to treat a fermionic system embedded in the effective external field produced by the spin-orbit coupling interaction. Even in the absence of a spin polarization, the SCDFT requires the electron-electron potential to depend on the spin currents \mathbf{J}^x , \mathbf{J}^y and \mathbf{J}^z , which only recently was made possible for practical relativistic quantum-mechanical simulations [Phys. Rev. B **102**, 235118 (2020)]. Here, we apply the SCDFT to the quantum spin-Hall phase and show how it improves (even qualitatively) the description of its electronic structure relative to the DFT. We study the Bi (001) 2D bilayer and its band insulator to topological insulator phase transition (via $s + p_z \leftrightarrow p_x + ip_y$ band inversion) as a function of mechanical strain. We show that the explicit account of spin currents in the electron-electron potential of the SCDFT is key to the appearance of a Dirac cone at the Γ point in the valence band structure at the onset of the topological phase transition. Finally, the valence band structure of this system is rationalized using a simple first-order $\mathbf{k} \cdot \mathbf{p}$ quasi-degenerate perturbation theory model.

INTRODUCTION

Quantum spin-Hall (QSH) systems (or topological insulators, TIs) are insulating in the bulk while they exhibit gapless edge states (ES) that hold spin currents with little or no dissipation. Notably, and in contrast to its relative (i.e. the quantum Hall phase), appearance of the conducting ES does not require breaking of time-reversal symmetry (TRS) [1–3]. Existence of the QSH phase was first proposed in the analytical model for graphene of Kane and Mele (KM) in 2005 from an inclusion of spin-orbit coupling (SOC) in the effective tight-binding Hamiltonian of Haldane [4, 5]. The same authors later showed that the QSH phase is in fact topologically distinct from other insulating states, being characterized by a \mathbb{Z}_2 topological invariant [6]. This implies that the conducting ES with desirable spin-transport properties are, in fact, particularly robust against perturbations.

Despite these early successes, the KM model is limited by the lack of renormalization of the SOC potential by the electron-electron (ee) interaction. At about the same time, Bencheikh showed how the spin current density functional theory (SCDFT) of Vignale and Rasolt [7] would provide a formulation of the DFT for a fermionic system in the effective external field produced by SOC [8]. It follows that the SCDFT provides the necessary theoretical framework to the description of the missing ee terms on the QSH phase. On the other hand, a conventional DFT treatment would not guarantee an accurate

description because its ee term does not satisfy certain invariance relations in the presence of SOC [9]. For TRS preserving states (such as those relevant to the QSH effect), the SCDFT dictates that the ee potential must depend on the electron density n , and on the three spin current densities \mathbf{J}^x , \mathbf{J}^y and \mathbf{J}^z [10–12]. The latter are exactly those physical quantities at the core of the peculiar transport phenomena in the QSH phase, and whose effect on the ee potential has been missing in previous treatments [13–21], with a notable exception being the study by Trushin and Görling of the AlBi and SnTe 3D TIs by use of the exact-exchange (EXX) functional [10]. With the latter approach, however, electron correlation is neglected. Some of the authors of this Letter have recently formulated a practical strategy to SCDFT calculations including the effects of electron correlation [11, 12, 22].

In this Letter, we apply the SCDFT to the QSH phase and show how the corresponding electronic structure differs even qualitatively from that predicted by the standard DFT. As a prototypical example, we study the band insulator to topological insulator phase transition in the Bi (001) 2D bilayer [13, 14, 19, 20, 23, 24]. We demonstrate that modification of the ee potential by the SOC-induced spin currents in SCDFT not only captures the expected band inversion phenomenon at the phase transition but also predicts the existence of previously overlooked Dirac fermions (DFs) emerging as quasiparticles close to the top of the valence band at the Γ point at the onset of the topological phase transition.

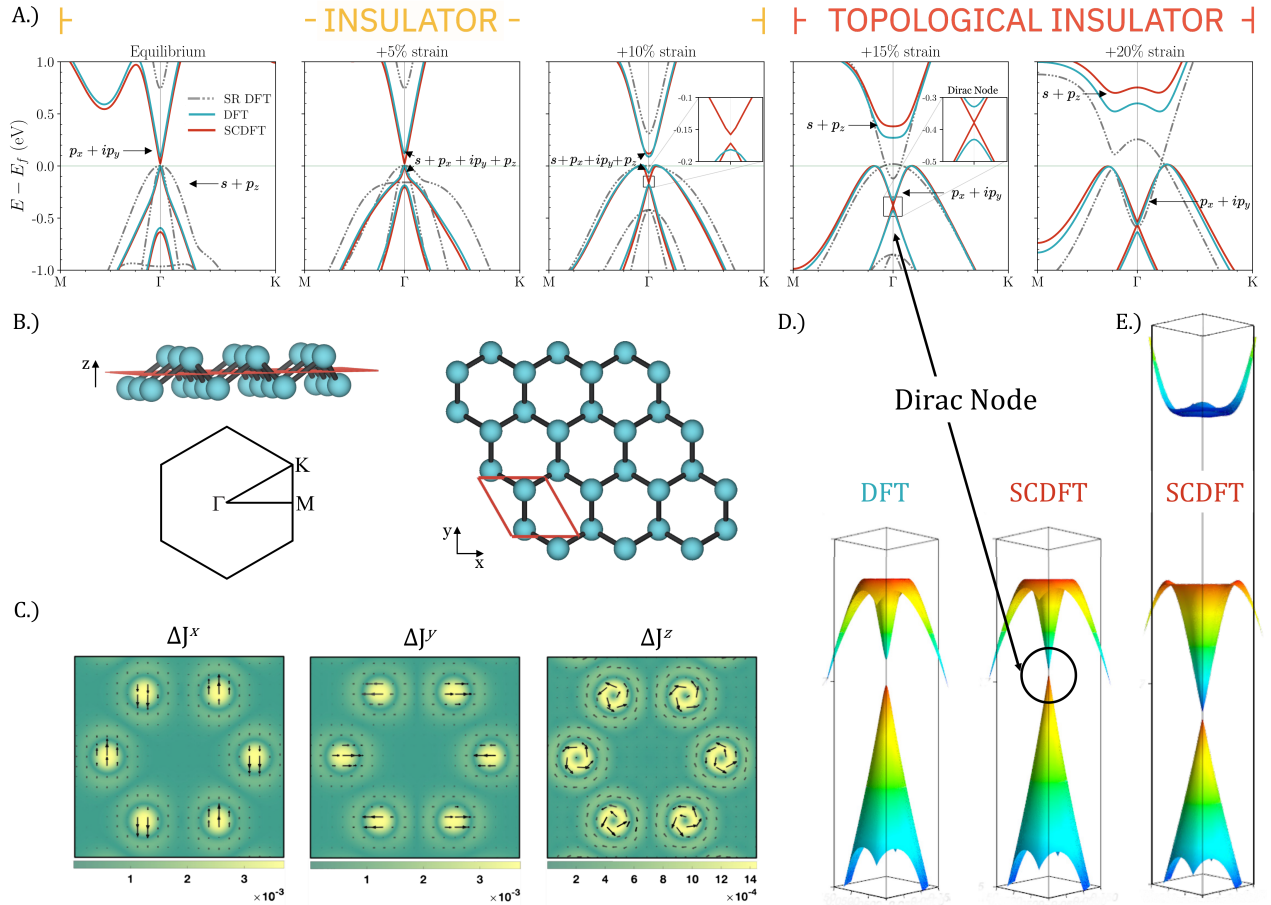


FIG. 1. Electronic structure of the Bi (001) bilayer as described by the DFT and SCDFE. A) Band structure along the $M - \Gamma - K$ path (shown to the right of the structure in B) as a function of strain (from the equilibrium lattice up to a +20% strain). Dashed black lines are from scalar-relativistic DFT (without SOC), blue continuous lines are from DFT with SOC (that is, from the potential of Eq. 2), and red continuous lines are from SCDFE with SOC (that is, from the potential of Eq. 1). The “character” of the top of valence and bottom of conduction bands in the vicinity of the Γ point is reported (in terms of the leading atomic orbital contributions). B) Atomic structure of the Bi (001) bilayer: side view (top) and top view (bottom). On the top, the plane between the two atomic layers is shown as a red plane. On the right the $M - \Gamma - K$ path is shown for the $R\bar{3}m$ space-group. C) Spin current densities \mathbf{J}^x , \mathbf{J}^y and \mathbf{J}^z for the +15% strain case in the plane highlighted in the top-left panel in B). The color identifies the absolute value in the selected plane while the length and direction of the superimposed black arrows represent the magnitude and direction of their in-plane Cartesian components. D) 3D representation of the top valence bands at +15% strain in the vicinity of Γ as obtained with the DFT (left) and SCDFE (right). E) 3D representation of the top valence bands and bottom conduction band in the vicinity of Γ at +20% strain as obtained with the SCDFE.

All calculations are performed with a developmental version of the CRYSTAL17 program [9, 25–28]. The computational details are reported in the electronic supporting information (ESI) [29] (see also Refs. [30–47] included therein). Our DFT and SCDFE calculations are based on hybrid exchange-correlation (xc) functionals, employing the generalized gradient approximation (GGA). Indeed, in the GGA of the SCDFE for TRS preserving electronic states, an adiabatic connection formula for the xc potential $\hat{v}_{xc}^{\text{SCDFE}}$ may be derived, by exploiting the short-range behaviour of the exchange hole, yield-

ing [11, 12, 48]:

$$\hat{v}_{xc}^{\text{SCDFE}}[n, \mathbf{J}^x, \mathbf{J}^y, \mathbf{J}^z] = \hat{v}_c[n] + (1 - \alpha) \hat{v}_x[n] + \alpha \hat{X}^{\text{SCDFE}}[n, \mathbf{J}^x, \mathbf{J}^y, \mathbf{J}^z], \quad (1)$$

where α is the dimensionless fraction of exact exchange (with its associated potential \hat{X}^{SCDFE}), and where \hat{v}_x and \hat{v}_c are exchange and correlation potentials in the GGA. On the other hand, in the DFT, the corresponding expression reads:

$$\hat{v}_{xc}^{\text{DFT}}[n] = \hat{v}_c[n] + (1 - \alpha) \hat{v}_x[n] + \alpha \hat{X}^{\text{DFT}}[n]. \quad (2)$$

The EXX potential \hat{X}^{DFT} in Eq. (2) may be obtained from a unitary transformation of \hat{X}^{SCDFE} , using an ap-

proach described in Ref. [12]. In Eq. (1), $\mathbf{J}^c(\mathbf{r})$ with $c = x, y, z$ are spin current densities defined as follows (for simplicity we report the expression for the one-electron non-periodic case):

$$\mathbf{J}^c(\mathbf{r}) = \frac{1}{2i} \{ \psi^\dagger(\mathbf{r}) \boldsymbol{\sigma}^c [\nabla \psi(\mathbf{r})] - [\nabla \psi^\dagger(\mathbf{r})] \boldsymbol{\sigma}^c \psi(\mathbf{r}) \}, \quad (3)$$

where $\psi(\mathbf{r})$ is a one-electron two-component (2c) spinor, $\boldsymbol{\sigma}^c$ is the c -th Pauli matrix and $i = \sqrt{-1}$. Therefore, a comparison of predictions from Eqs. (1) and (2) provides a probe to study the effect on the electronic structure of including the spin current densities in the ee potential. Here, the xc GGA potential is PBE and $\alpha = 10\%$.

Starting from the conventional rhombohedral $R\bar{3}m$ bulk crystal structure of Bi [49], we extract a 2D layered structure by cutting over a plane orthogonal to the [001] direction, leading to a buckled-honeycomb bilayer shown in Figure 1B. Then, we fully relax the structure (in terms of both lattice parameters and atomic positions) at the scalar-relativistic (SR) level, under the only constraints provided by the hexagonal layer group symmetry. Strained configurations are explored by constraining the lattice parameters to larger values compared to the equilibrium ones (+5, +10, +15 and +20%) and by letting the atoms relax within the strained cells.

The evolution of the electronic band structure as a function of strain is reported in Figure 1A as predicted by scalar relativistic (SR) calculations (i.e. without SOC) and by inclusion of SOC within a DFT and SCDFE framework. For the Bi (001) bilayer, the bands are constrained both by TRS [$\epsilon^\dagger(\mathbf{k}) = \epsilon^\dagger(-\mathbf{k})$] and space-inversion symmetry [$\epsilon^\dagger(\mathbf{k}) = \epsilon^\dagger(-\mathbf{k})$] leading to $\epsilon^\dagger(\mathbf{k}) = \epsilon^\dagger(\mathbf{k})$, such that the bands are doubly-degenerate and SOC-induced spin-splitting does not occur. The DFT bands resulting from calculations with $\alpha = 0$ are also provided in Fig. S1 of the ESI.

At the equilibrium structure (Figure 1A, leftmost panel), the effect of SOC is manifested through the drastic reduction of the direct band gap at Γ (from 0.75 eV to 0.02 eV), as already noted from previous DFT calculations [15]. Moving to the right panels, as the lattice parameter is expanded, a typical band-inversion (BI) profile is observed. The BI can be tracked through an analysis of the principal atomic-orbital components of the crystalline single-particle orbitals at Γ . At the equilibrium configuration, the top of the valence band is of mixed $s + p_z$ character, while the bottom of the conduction band is of the type $p_x + ip_y$. As the lattice is expanded, these components are initially mixed in both states (see +5% and +10% strained configurations) and eventually inverted at +15% strain, a typical signature of the topological phase transition (TPT) [1, 21, 50]. We also note that, at the TPT, the band gap opens significantly.

Remarkably, at the onset of the TPT (i.e. at +15% strain), the SCDFE predicts the formation of a doubly-degenerate Dirac cone (DC) at the top of the valence

band at Γ , which is not predicted by the DFT (see Figure 1A and 1D). That is, the formation of such a distinctive electronic feature is only predicted by inclusion of the spin current densities in the ee potential. Even more remarkably, this same DC was noted in previous angle-resolved photoemission spectroscopy experiments, but was attributed as being due to the interaction with the substrate [23].

We rationalize the formation of this DC by means of a first-order $\mathbf{k} \cdot \mathbf{p}$ quasi-degenerate perturbation theory model of the valence band structure, inspired by Kane's model [51, 52]. Formal aspects are given in the ESI. We show that when the SOC-induced gap at the Γ point, E_Γ , is large, the model predicts a dispersion relation for the four highest-lying valence bands exactly along a doubly-degenerate DC:

$$\epsilon(\mathbf{k}) = \pm v|\mathbf{k}|, \quad (4)$$

where v is the band velocity. Thus, the formation of the DC by the SCDFE correlates with the larger SOC-induced gap of $E_\Gamma = 0.40$ eV compared to that of

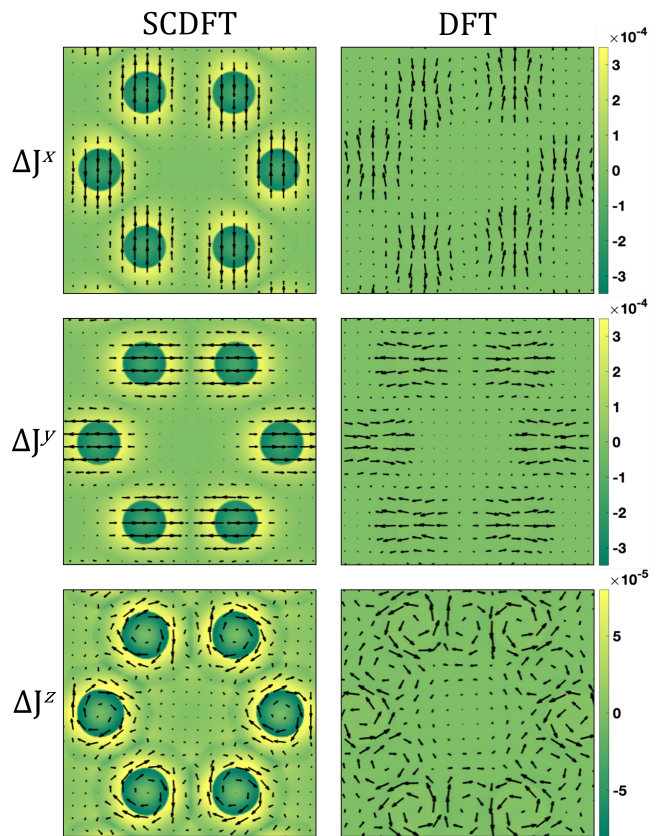


FIG. 2. Effect of orbital-relaxation through the self-consistent field process on spin current densities in DFT and SCDFE calculations. The reported quantities are differences between the final electronic solution and the initial one: $\Delta \mathbf{J}^c = \mathbf{J}_{\text{final}}^c - \mathbf{J}_{\text{initial}}^c$, with $c = x, y, z$. The panels show color maps of the spatial distribution of these quantities in the same plane as in Figure 1C.

$E_{\Gamma} = 0.28$ eV by the DFT where the DC does not emerge. As discussed above, this is entirely due to the dependence on the three spin current densities \mathbf{J}^x , \mathbf{J}^y and \mathbf{J}^z of the SCDFT ee potential of Eq. (1). Figure 1C shows the spatial distribution of these vector quantities in the central plane of the Bi (001) bilayer.

The leading effect of including the three spin current densities in the ee potential has been discussed above and is further highlighted and quantified below. Let us stress that, in the presence of SOC, spin current densities can be computed from Eq. (3) both within a DFT and SCDFT approach. However, we show in Figure 2 that their inclusion in the ee potential in the SCDFT case results in their significant evolution along the self-consistent field process (i.e. orbital relaxation), which, on the other hand, is lacking in the DFT. Figure 2 shows color maps of the orbital relaxation of the three spin current densities along the SCF: $\Delta\mathbf{J}^c = \mathbf{J}_{\text{final}}^c - \mathbf{J}_{\text{initial}}^c$, with $c = x, y, z$, where the initial quantities are calculated from a second-variational treatment of SOC (i.e. after a single diagonalization of the $2c$ Hamiltonian built from SR orbitals). The color scale describes the magnitude of the quantities while the arrows represent their local orientation and magnitude in the selected plane (same as in Figure 1). The figure clearly shows that DFT calculations are incapable of accounting for the orbital-relaxation of the spin currents. On the other hand, the SCDFT calculation allows for the significant build-up of spin currents along the SCF process. Ultimately, this enhanced role of the spin currents in the SCDFT compared to the DFT is at the core of the formation of the DC in the valence bands of the Bi (001) bilayer at the onset of the TPT.

Acknowledgments This work was supported in part through computational resources and services provided by the Institute for Cyber-Enabled Research at Michigan State University. J.K.D. is grateful to the National Science and Engineering Research Council of the Government of Canada for a Postdoctoral Fellowship application # 545643. We are grateful to John S. Tse for a fruitful discussion.

* alessandro.erba@unito.it

† jmendoza@msu.edu

‡ jacqueskontak.desmarais@unito.it

- [1] B. A. Bernevig, T. L. Hughes, and S.-C. Zhang, Quantum spin hall effect and topological phase transition in hgte quantum wells, *Science* **314**, 1757 (2006).
- [2] J. E. Moore, The birth of topological insulators, *Nature* **464**, 194 (2010).
- [3] C. L. Kane and E. J. Mele, A new spin on the insulating state, *Science* **314**, 1692 (2006).
- [4] C. L. Kane and E. J. Mele, Quantum spin hall effect in graphene, *Phys. Rev. Lett.* **95**, 226801 (2005).
- [5] F. D. M. Haldane, Model for a quantum hall effect without landau levels: Condensed-matter realization of the "parity anomaly", *Phys. Rev. Lett.* **61**, 2015 (1988).
- [6] C. L. Kane and E. J. Mele, Z 2 topological order and the quantum spin hall effect, *Phys. Rev. Lett.* **95**, 146802 (2005).
- [7] G. Vignale and M. Rasolt, Current-and spin-density-functional theory for inhomogeneous electronic systems in strong magnetic fields, *Phys. Rev. B* **37**, 10685 (1988).
- [8] K. Bencheikh, Spin-orbit coupling in the spin-current-density-functional theory, *J. Phys. A* **36**, 11929 (2003).
- [9] J. K. Desmarais, J.-P. Flament, and A. Erba, Spin-orbit coupling in periodic systems with broken time-reversal symmetry: Formal and computational aspects, *Phys. Rev. B* **101**, 235142 (2020).
- [10] E. Trushin and A. Görling, Spin-current density-functional theory for a correct treatment of spin-orbit interactions and its application to topological phase transitions, *Phys. Rev. B* **98**, 205137 (2018).
- [11] J. K. Desmarais, J.-P. Flament, and A. Erba, Adiabatic connection in spin-current density functional theory, *Phys. Rev. B* **102**, 235118 (2020).
- [12] F. Bodo, J. K. Desmarais, and A. Erba, Spin current density functional theory of weyl semimetals, *Phys. Rev. B* **105**, 125108 (2022).
- [13] T. Hirahara, T. Nagao, I. Matsuda, G. Bihlmayer, E. Chulkov, Y. M. Koroteev, P. Echenique, M. Saito, and S. Hasegawa, Role of spin-orbit coupling and hybridization effects in the electronic structure of ultrathin bi films, *Phys. Rev. Lett.* **97**, 146803 (2006).
- [14] Y. M. Koroteev, G. Bihlmayer, J. Gayone, E. V. Chulkov, S. Blügel, P. M. Echenique, and P. Hofmann, Strong spin-orbit splitting on bi surfaces, *Phys. Rev. Lett.* **93**, 046403 (2004).
- [15] I. Yakovkin, Dependence of the band structure of bi(111) bilayers on lattice constant and spin-orbit splitting induced by a h monolayer, *Journal of Physics and Chemistry of Solids* **129**, 277 (2019).
- [16] Y. Xia, D. Qian, D. Hsieh, L. Wray, A. Pal, H. Lin, A. Bansil, D. Grauer, Y. S. Hor, R. J. Cava, *et al.*, Observation of a large-gap topological-insulator class with a single dirac cone on the surface, *Nat. Phys.* **5**, 398 (2009).
- [17] D. Hsieh, D. Qian, L. Wray, Y. Xia, Y. S. Hor, R. J. Cava, and M. Z. Hasan, A topological dirac insulator in a quantum spin hall phase, *Nature* **452**, 970 (2008).
- [18] H. Zhang, C.-X. Liu, X.-L. Qi, X. Dai, Z. Fang, and S.-C. Zhang, Topological insulators in bi2se3, bi2te3 and sb2te3 with a single dirac cone on the surface, *Nat. Phys.* **5**, 438 (2009).
- [19] S. Murakami, Quantum spin hall effect and enhanced magnetic response by spin-orbit coupling, *Phys. Rev. Lett.* **97**, 236805 (2006).
- [20] M. Wada, S. Murakami, F. Freimuth, and G. Bihlmayer, Localized edge states in two-dimensional topological insulators: Ultrathin bi films, *Phys. Rev. B* **83**, 121310 (2011).
- [21] S. Chege, P. Ning'i, J. Sifuna, and G. O. Amolo, Origin of band inversion in topological bi2se3, *AIP Advances* **10**, 095018 (2020).
- [22] J. K. Desmarais, J.-P. Flament, and A. Erba, Fundamental role of fock exchange in relativistic density functional theory, *J. Phys. Chem. Lett.* **10**, 3580 (2019).
- [23] F. Yang, L. Miao, Z. Wang, M.-Y. Yao, F. Zhu, Y. Song, M.-X. Wang, J.-P. Xu, A. V. Fedorov, Z. Sun, *et al.*, Spatial and energy distribution of topological edge states in single bi (111) bilayer, *Phys. Rev. Lett.* **109**, 016801 (2012).

- (2012).
- [24] I. K. Drozdov, A. Alexandradinata, S. Jeon, S. Nadj-Perge, H. Ji, R. Cava, B. Andrei Bernevig, and A. Yazdani, One-dimensional topological edge states of bismuth bilayers, *Nat. Phys.* **10**, 664 (2014).
- [25] R. Dovesi, A. Erba, R. Orlando, C. M. Zicovich-Wilson, B. Civalleri, L. Maschio, M. Rérat, S. Casassa, J. Baima, S. Salustro, and B. Kirtman, Quantum-mechanical condensed matter simulations with CRYSTAL, *Wiley Interdisciplinary Reviews: Computational Molecular Science* **8**, 1 (2018).
- [26] A. Erba, J. Baima, I. Bush, R. Orlando, and R. Dovesi, Large scale condensed matter dft simulations: Performance and capabilities of the CRYSTAL code, *J. Chem. Theory Comput.* **13**, 5019 (2017).
- [27] J. K. Desmarais, J.-P. Flament, and A. Erba, Spin-orbit coupling from a two-component self-consistent approach. i. generalized hartree-fock theory, *J. Chem. Phys.* **151**, 074107 (2019).
- [28] J. K. Desmarais, S. Komorovsky, J.-P. Flament, and A. Erba, Spin-orbit coupling from a two-component self-consistent approach. ii. non-collinear density functional theories, *J. Chem. Phys.* **154**, 204110 (2021).
- [29] See Supplemental Material at URL for computational details, for presentation of the analytical quasi-degenerate perturbation theory model, and for bands from pure-GGA calculations (without exact exchange).
- [30] K. Doll, V. Saunders, and N. Harrison, Analytical hartree-fock gradients for periodic systems, *Int. J. Q. Chem.* **82**, 1 (2001).
- [31] K. Doll, Implementation of analytical hartree-fock gradients for periodic systems, *Comput. Phys. Commun.* **137**, 74 (2001).
- [32] K. Doll, R. Dovesi, and R. Orlando, Analytical hartree-fock gradients with respect to the cell parameter: systems periodic in one and two dimensions, *Theor. Chem. Acc.* **115**, 354 (2006).
- [33] B. Civalleri, P. D'Arco, R. Orlando, V. Saunders, and R. Dovesi, Hartree-fock geometry optimisation of periodic systems with the crystal code, *Chem. Phys. Lett.* **348**, 131 (2001).
- [34] B. Metz, H. Stoll, and M. Dolg, Small-core multiconfiguration-dirac-hartree-fock-adjusted pseudopotentials for post-d main group elements: Application to pbh and pbo, *J. Chem. Phys.* **113**, 2563 (2000).
- [35] E. Heifets, E. Kotomin, A. Bagaturyants, and J. Maier, Ab initio study of bifeo₃: thermodynamic stability conditions, *J. Phys. Chem. Lett.* **6**, 2847 (2015).
- [36] V. I. Lebedev, Quadratures on a sphere, *USSR Comput. Math. Math. Phys.* **16**, 10 (1976).
- [37] V. I. Lebedev, Spherical quadrature formulas exact to orders 25–29, *Sib. Math. J.* **18**, 99 (1977).
- [38] M. D. Towler, A. Zupan, and M. Causà, Density functional theory in periodic systems using local gaussian basis sets, *Comput. Phys. Commun.* **98**, 181 (1996).
- [39] J. P. Perdew, K. Burke, and M. Ernzerhof, Generalized gradient approximation made simple, *Phys. Rev. Lett.* **77**, 3865 (1996).
- [40] A. Seidl, A. Görling, P. Vogl, J. A. Majewski, and M. Levy, Generalized kohn-sham schemes and the band-gap problem, *Phys. Rev. B* **53**, 3764 (1996).
- [41] A. Görling and M. Levy, Exact kohn-sham scheme based on perturbation theory, *Phys. Rev. A* **50**, 196 (1994).
- [42] J. P. Perdew, M. Ernzerhof, and K. Burke, Rationale for mixing exact exchange with density functional approximations, *J. Chem. Phys.* **105**, 9982 (1996).
- [43] C. Adamo and V. Barone, Toward reliable density functional methods without adjustable parameters: The pbe0 model, *J. Chem. Phys.* **110**, 6158 (1999).
- [44] J. Heyd, G. E. Scuseria, and M. Ernzerhof, Hybrid functionals based on a screened coulomb potential, *J. Chem. Phys.* **118**, 8207 (2003).
- [45] R. Dick, *Advanced quantum mechanics* (Springer, 2012).
- [46] L. C. L. Y. Voon and M. Willatzen, *The kp method: electronic properties of semiconductors* (Springer Science & Business Media, 2009).
- [47] B. Kirtman, Simultaneous calculation of several interacting electronic states by generalized van vleck perturbation theory, *J. Chem. Phys.* **75**, 798 (1981).
- [48] S. Pittalis, G. Vignale, and F. Eich, U (1) × su (2) gauge invariance made simple for density functional approximations, *Phys. Rev. B* **96**, 035141 (2017).
- [49] Z. Wei, C. Dubceac, M. A. Petrukhina, and E. V. Dikarev, From a volatile molecular precursor to twin-free single crystals of bismuth, *Chem. Commun.* **55**, 5717 (2019).
- [50] J. Maciejko, T. L. Hughes, and S.-C. Zhang, The quantum spin hall effect, *Annu. Rev. Condens. Matter Phys.* **2**, 31 (2011).
- [51] E. O. Kane, Band structure of indium antimonide, *J. Phys. Chem. Solids* **1**, 249 (1957).
- [52] M. Orlita, D. Basko, M. Zholudev, F. Teppe, W. Knap, V. Gavrilenko, N. Mikhailov, S. Dvoretzkii, P. Neugebauer, C. Faugeras, *et al.*, Observation of three-dimensional massless kane fermions in a zinc-blende crystal, *Nat. Phys.* **10**, 233 (2014).